

## A POD-Based Variational Multiscale Method for Large Eddy Simulation of Turbulent Channel Flows

Chen, L.; Hu, Xu Qu

**DOI**

[10.1142/S0219876217500499](https://doi.org/10.1142/S0219876217500499)

**Publication date**

2016

**Document Version**

Final published version

**Published in**

International Journal of Computational Methods

**Citation (APA)**

Chen, L., & Hu, X. Q. (2016). A POD-Based Variational Multiscale Method for Large Eddy Simulation of Turbulent Channel Flows. *International Journal of Computational Methods*, 14(5).  
<https://doi.org/10.1142/S0219876217500499>

**Important note**

To cite this publication, please use the final published version (if applicable).  
Please check the document version above.

**Copyright**

Other than for strictly personal use, it is not permitted to download, forward or distribute the text or part of it, without the consent of the author(s) and/or copyright holder(s), unless the work is under an open content license such as Creative Commons.

**Takedown policy**

Please contact us and provide details if you believe this document breaches copyrights.  
We will remove access to the work immediately and investigate your claim.

# A POD-Based Variational Multiscale Method for Large Eddy Simulation of Turbulent Channel Flows

Lin-Feng Chen

*State Key Laboratory of Advanced Design  
and Manufacturing for Vehicle Body  
Hunan University, Changsha 410082, P. R. China  
Aerospace Engineering, Delft University of Technology  
Kluyverweg 1 Delft, 2629 HS, The Netherlands  
Lnfnqchn@gmail.com*

Xu-Qu Hu\*

*State Key Laboratory of Advanced Design  
and Manufacturing for Vehicle Body  
College of Mechanical and Vehicle Engineering  
Hunan University, Changsha 410082, P. R. China  
huxuqu@gmail.com*

Received 4 September 2016

Revised 26 September 2016

Accepted 28 September 2016

Published 1 November 2016

A POD-based variational multiscale method (VMM) for large eddy simulation (LES) of turbulent channel flows is proposed. The incompressible Navier–Stokes equations are solved using a residual-based VMM technique, and the residual-based model coefficient is adopted from Taylor *et al.* [1998] “Finite element modeling of blood flow in arteries,” *Comput. Methods in Appl. Mech. Eng.* **158**(1–2), 155–196. A generalized- $\alpha$  method is applied for the temporal integration. Numerical results show that four or higher wall-normal modes need to be applied for reproducing most of the turbulent characteristics. Results of large vortex structures and the low velocity streaks prove that the turbulent channel flows are well estimated by the proposed approach. The statistical analysis of the turbulent velocities confirms its reliability in turbulent channel flows.

*Keywords:* Variational multiscale method; proper orthogonal decomposition; turbulent channel flow.

## 1. Introduction

Turbulent flow exists widely in nature and industry, for which a precise solution is hard to be determined not only because time-dependent phenomena are involved,

\*Corresponding author.

but it also relates to high-dimensional data and variational multiscale problems [Moin and Moser (1989); Wei and Hu (2016)].

The high-dimensional dataset can be degraded to get a low-dimensional model by the reduced order model (ROM) technique, which allows the possibility to capture most of the phenomena in the original dimensions. The ROM based on a proper orthogonal decomposition (POD), also known as Karhunen–Loeve decomposition, has been widely used to obtain low-dimensional descriptions of turbulent systems. One of the earliest applications of POD modes in turbulence was implemented by Lumley [1967]. It provided an objective, energy-based criterion to help identify key motions in the turbulent flows, which stands as a bridge between the mathematical systems and the empirical quest for coherent structures. This approach was also applied to analyze turbulent flow characteristics by constructing low-dimensional models [Lumley (1967); Moin and Moser (1989); Aubry *et al.* (1988); Amsallem *et al.* (2009)]. Bakewell *et al.* measured two-point correlations of one velocity component in the wall region of a fully developed turbulent pipe flow, and reconstructed the two-point correlation tensor using incompressibility and a closure assumption [Bakewell and Lumley (1967)]. A dominant large-scale structure of the flow in the wall region, obtained with the aid of a mixing length approximation, was consisted of randomly distributed counter-rotating eddy pairs of elongated streamwise extent. Moin *et al.* successfully performed a comprehensive POD analysis based on a flow data base [Moin and Moser (1989)]. They proved that coherent structures can be extracted by decomposing the velocity into characteristic eddies, which dominate the production of important statistics. The POD modes were also computed from a similar direct numerical simulation (DNS) of channel flow in Sirovich [1991] and Ball *et al.* [1991], in which the temporal behavior of the coefficients  $a_k(t)$  of the empirical eigenfunction were extracted directly from numerical database. The obtained time series showed strong intermittency, as one would expect from the experimental observations of the bursting process.

Theoretically speaking, the solution to the variational multiscale problem in turbulence can be decomposed into the resolved and unresolved scales, as  $u = \bar{u} + u'$ . The variational multiscale method (VMM) is a consistent approach to account for the effects of unresolved scales on computing numerical solutions [Hughes and Sangalli (2007)]. Simplified equations for the resolved problem of  $\bar{u}$  can be achieved by eliminating the unresolved scale  $u'$  through analytical derivations. The simplified resolved equations using the VMM was initially integrated to the large eddy simulation (LES) in Hughes *et al.* [2000], which can be called by VMM-LES technique. The VMM-LES technique decomposes the solution space of the Navier–Stokes equations into large, small and unresolved scales. In pioneering studies, the effect of unresolved scales on the large-scale equations was ignored, and a Smagorinsky type model in the small-scale equations was introduced to account for the dissipation of “missing small scales” [Hughes *et al.* (2001a,b)]. Lately, a single model for the effect of unresolved scales was applied to the resolved-scale equations [Calo (2005); Bazilevs *et al.* (2007)]. Previous work demonstrates that the numerical results obtained by

VMM-LES technique coincide well with experimental observations of variational multiscale turbulent phenomena.

Although the high-dimensional and variational multiscale problems in turbulent flows can be individually considered by the POD and VMM-LES techniques, the comprehensive studies on the joint effect of this two properties are still not easily available. Some progress has been done on this topic. For example, Wang *et al.* tested four closure models for the POD-based ROM of structurally dominated turbulent flows past a circular cylinder. They showed that the dynamic unresolved-scale and the variational multiscale models resulted in the best accuracy with a high level of computational efficiency [Wang *et al.* (2012)]. In our previous study, the POD was applied to construct small scales using VMM for a stochastically forced Burgers problem [Chen *et al.* (2015)]. The numerical implementation with the VMM model was proven to be able to avoid the stability issue, which exists in most applications of POD. However, its applications in turbulent flows still need to be progressed, which becomes the initiation of present study.

In this paper, we construct the small-scale models in the variational multiscale formulations for the LES of turbulent channel flow by using truncated sets of POD modes (Sec. 2). The simplified resolved equations by VMM-LES technique was solved to examine the feasibility of the application of POD-based VMM-LES. Results and discussions about amplitudes of POD modes, vortex structure and statistical analysis are presented in Sec. 3. Conclusions and perspectives of this study are summarized in Sec. 4.

## 2. Methods and Models

### 2.1. VMM for Navier–Stokes equations

As shown in Fig. 1, the turbulent flows at  $\text{Re}_\tau = 180$  is considered in a rectangular channel of  $L_x = 6$ ,  $L_y = 2$  and  $L_z = 4$ . The Reynolds number  $\text{Re}_\tau = u_\tau \delta / \nu$ , where  $u_\tau = \sqrt{\tau / \rho}$  is friction velocity, which is based on wall shear stress  $\tau$  and density  $\rho$ ,  $\delta$  is half the channel thickness and  $\nu$  is the kinematic viscosity. The turbulent channel flow can be described by the incompressible Navier–Stokes equations,

$$\frac{\partial \mathbf{u}}{\partial t} + \nabla \cdot (\mathbf{u} \otimes \mathbf{u}) + \nabla p - \nabla \cdot 2\nu \nabla^s \mathbf{u} = \mathbf{f}, \quad \text{in } \Omega, \quad (1)$$

$$\nabla \cdot \mathbf{u} = 0, \quad \text{in } \Omega, \quad (2)$$

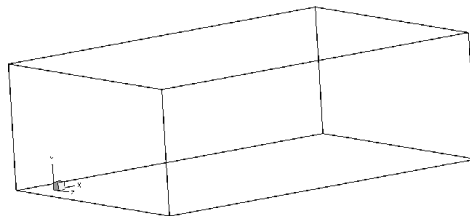


Fig. 1. Sketch of turbulent channel flows with numerical domain of ( $L_x = 6$ ,  $L_y = 2$ ,  $L_z = 4$ ).

where  $\mathbf{u}$  represents velocities in turbulent flows,  $p$  denotes the pressure,  $\mathbf{f}$  is the body force and  $\Omega$  denotes the computational domain of the channel. The symmetric velocity gradient is defined by  $\nabla^s \mathbf{u} = \frac{1}{2}(\nabla \mathbf{u} + \nabla \mathbf{u}^T)$ .

The variational form of the incompressible Navier–Stokes equations is obtained by taking the inner product of weighting functions  $\mathbf{W} = \{\mathbf{w}, q\}^T$  with the strong form (Eqs. (1) and (2)) and integrating over the space–time domain,  $Q$ . Doing so yields a weak or variational form of the Navier–Stokes equations

$$\left( \mathbf{w}, \frac{\partial \mathbf{u}}{\partial t} \right) - (\nabla \mathbf{w}, \mathbf{u} \otimes \mathbf{u}) + (q, \nabla \cdot \mathbf{u}) - (\nabla \cdot \mathbf{w}, p) + (\nabla^s \mathbf{w}, 2\nu \nabla^s \mathbf{u}) = (\mathbf{w}, F), \quad (3)$$

where  $(\cdot, \cdot)$  represents an integration in the space domain,  $\mathbf{w}$  and  $q$  represent weighting functions corresponding to  $\mathbf{u}$  and  $p$ , respectively.

Decomposing the weighting and solution spaces into resolved  $(\bar{\mathbf{W}}, \bar{\mathbf{U}})$  and unresolved  $(\mathbf{W}', \mathbf{U}')$  scales, and neglecting the unresolved-scale system yields the resolved-scale equations

$$\begin{aligned} & \left( \bar{\mathbf{w}}, \frac{\partial \bar{\mathbf{u}}}{\partial t} \right) - (\nabla \bar{\mathbf{w}}, \bar{\mathbf{u}} \otimes \bar{\mathbf{u}}) + (\bar{q}, \nabla \cdot \bar{\mathbf{u}}) - (\nabla \cdot \bar{\mathbf{w}}, \bar{p}) + (\nabla^s \bar{\mathbf{w}}, 2\nu \nabla^s \bar{\mathbf{u}}) \\ & - (\nabla \bar{\mathbf{w}}, \bar{\mathbf{u}} \otimes \mathbf{u}') - (\nabla \bar{\mathbf{w}}, \mathbf{u}' \otimes \bar{\mathbf{u}}) - (\nabla \bar{\mathbf{w}}, \mathbf{u}' \otimes \mathbf{u}') + (\bar{q}, \nabla \cdot \mathbf{u}') \\ & - (\nabla \cdot \bar{\mathbf{w}}, p') = (\mathbf{w}, \mathbf{f}), \end{aligned} \quad (4)$$

where the large scales depend on  $\{\mathbf{u}', p'\}$ .

The simulation is carried out in a rectangular channel  $\Omega = [0 \ L_x] \times [0 \ L_y] \times [0 \ L_z]$ . The flow is driven by a constant force. The coordinate directions  $x$ ,  $y$ ,  $z$ , following the usual convention, are aligned with the streamwise, wall-normal and spanwise directions, respectively. The velocity components are likewise denoted  $\mathbf{u} = \{u, v, w\}$ . The boundary conditions are periodic in  $x$ - and  $z$ -directions, and no-slip at  $y = 0$  and  $y = L_y$ . The problem configuration is schematically illustrated in Fig. 1. In the calculation of the integration in space, a Gauss quadrature rule is applied. The variational equations above are advanced in time using a second-order generalized- $\alpha$  method.

## 2.2. POD small-scale modes for resolved-scale equations

### 2.2.1. Preparation of reference data

In order to produce reference data for the POD, a simulation of the channel flow case was carried out using a finite-volume method. A summary of simulation parameters are listed in Table 1.

The Navier–Stokes equations were solved using variant of channelFoam solver of OpenFOAM software package modified to include the forcing. For time integration a second-order backward scheme (BDF2) is used, and for space the central differencing (second-order) is used.

Table 1. Summary of simulation parameters at  $\text{Re}_\tau = 180$ .

Description	Symbol	Value
Domain size	$L_x \times L_y \times L_z$	$6 \times 2 \times 4$
Number of cells	$n_x \times n_y \times n_z$	$128 \times 128 \times 128$
Cell size	$h_x$	$L_x/n_x = 4.69 \times 10^{-2}$
First cell $y^+$	$y_1^+$	1.4
Fluid viscosity	$\nu$	$1/\text{Re} = 5.56 \times 10^{-3}$
Volumetric body force	$f$	1
Courant number	$C_o$	0.4
Bulk velocity	$U_{\text{bulk}}$	$\approx 15.5$
Maximum velocity	$U_{\text{max}}$	$\approx 20$
Time step	$\Delta t$	$\frac{C_{ohx}}{U_{\text{max}}} \approx 0.94 \times 10^{-3}$
Simulation time	$T$	200
Snapshot interval	$t_s$	0.25
Number of snapshots	$n_s$	800

In the simulation a homogeneous dynamic Smagorinsky SGS model is used with van Driest delta with default parameters. Homogeneous here means that the Smagorinsky coefficient is averaged over the whole domain.

First the preliminary simulation was run starting with parabolic profile perturbed with random values. This simulation is run for sufficient time for turbulence to develop fully. The result of the preliminary simulation is used as an initial condition for the main simulation.

The simulation is run for 200 time units to generate data for the POD. Snapshots of the velocity (and later pressure) fields are stored every 0.25 time units. A comparison of statistics between present and Jimenez's simulations [Jimenez and Moser (2007)] is carried out (Fig. 2). It shows statistics by the present simulation are in a good agreement with Jimenez's.

### 2.2.2. Construction of POD small-scale modes

The starting point of the procedure is the decomposition of the velocity  $u$  into its mean and fluctuating part

$$u = U + \tilde{u}, \quad (5)$$

where  $U$  is the horizontally averaged, time-dependent velocity.

Application of the POD theorem to turbulent channel flow with one direction of flow inhomogeneity and two homogeneous directions can be found in Lumley [1967] and Moin and Moser [1989]. A similar approach is used here, which is described below. The Karhunen–Loeve expansion (or POD) requires the two-point correlation tensor of fluctuations,

$$R_{ij}(r_x, y, y', r_z) = \langle \tilde{u}_i(x, y, z, t) \tilde{u}_j(x + r_x, y', z + r_z, t) \rangle, \quad (6)$$

where  $\tilde{u}_i$  ( $i = 1, 2, 3$ ) are the instantaneous turbulent velocity fluctuations in the streamwise,  $x$ , normal,  $y$ , and spanwise,  $z$ , directions, respectively. The  $\langle \rangle$  denotes

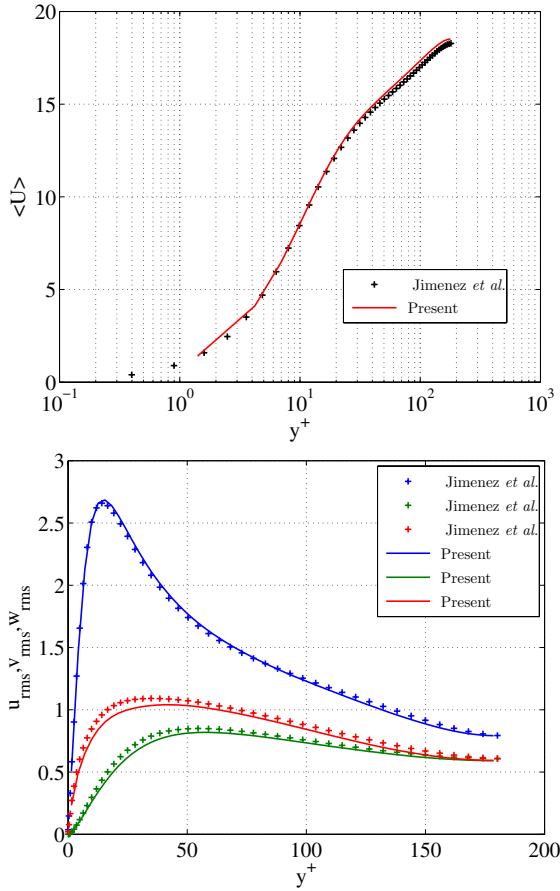


Fig. 2. Profiles of mean velocity  $\langle U \rangle$  and root-mean-square (RMS) of fluctuating velocities  $\{u_{rms}, v_{rms}, w_{rms}\}$  versus  $y^+ = u_\tau y / \nu$ .

ensemble average which, owing to flow homogeneity in  $x$ - and  $z$ -directions, is calculated by averaging in  $xz$ -plane as well as in time. It is actually more convenient to compute and use the two-point spectral-density tensor  $\Phi_{ij}(k_x, y, y', k_z)$  which is the Fourier transform of the two-point correlation tensor in  $r_x$  and  $r_z$ , that is

$$\Phi_{ij}(k_x, y, y', k_z) = \int \int e^{-ik_x r_x - ik_z r_z} R_{ij}(r_x, y, y', r_z) dr_x dr_z, \quad (7)$$

where  $k_x$  and  $k_z$  are the wave numbers in the  $x$ - and  $z$ -directions.

For computational purposes, the discrete Fourier transform of each instantaneous velocity field has been computed as

$$\hat{u}_i(k_x, y, k_z, t_n) = \sum_{x,z} \tilde{u}_i(k_x, y, k_z, t_n) e^{-ik_x x - ik_z z}. \quad (8)$$

The two-point spectral density is obtained from

$$\Phi_{ij}(k_x, y, y', k_z) = \frac{1}{N_t} \sum_{n=1}^{N_t} \hat{u}_i(k_x, y, k_z, t_n) \hat{u}_j^*(k_x, y', k_z, t_n), \quad (9)$$

where  $N_t$  is the number of instantaneous flow fields used for ensemble averaging and  $*$  denotes complex conjugate.

Then the Karhunen–Loeve expansion leads to an algebraic eigenvalue and eigenfunction problem of the two-point correlation tensor,

$$\mathbf{A}\phi^{(n)} = \lambda^{(n)} \phi^{(n)}, \quad (10)$$

where  $\mathbf{A}$  is the two-point correlation tensor, a  $3N \times 3N$  matrix ( $N$  is the number of discrete grid points in the normal direction) and

$$\phi^{(n)} = [\phi_1^{(n)}(1), \phi_2^{(n)}(1), \phi_3^{(n)}(1), \dots, \phi_1^{(n)}(N), \phi_2^{(n)}(N), \phi_3^{(n)}(N),]^T \quad (11)$$

is the discretized  $n$ th eigenvector (of dimension  $3N$ ), with  $\phi_1^{(n)}(i)$  the streamwise component of the  $n$ th eigenfunction at the  $i$ th grid point.

The eigenvalues are arranged in descending order with  $\lambda^{(1)}$  as the largest eigenvalue. Hereafter we denote  $l, k$  as the streamwise and spanwise wavenumber index. The first six eigenfunctions for the entire normal domain at  $l = 0, k = 2$  are shown in Fig. 3. Note that the eigenfunctions in the entire normal domain occur in pairs and are closely symmetric at the centerline. Additionally, the Karhunen–Loeve eigenfunctions behave in the same manner as other typical eigenfunctions, namely, the number of zero-crossing increases with the order of the eigenfunctions. Here it is particularly significant that the streamwise,  $\phi_1^{(n)}$ , and vertical,  $\phi_2^{(n)}$ , components have opposite (same) signs near the bottom (top) boundary, by which they make a positive contribution to turbulence production (Reynolds stress).

Figure 4 shows profiles of eigenvalues and energy percentage versus the order of the eigenmode at ( $l = 0, k = 2$ ). Note that energy is concentrated into the

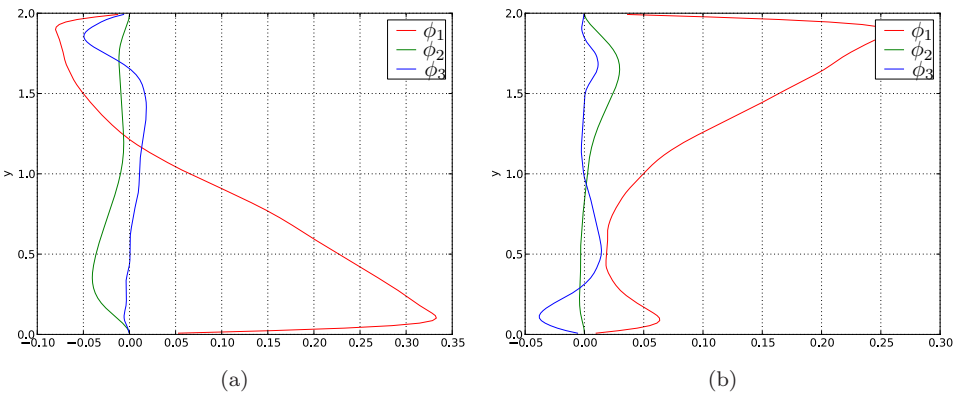


Fig. 3. The first six eigenfunctions  $\{\phi_1, \phi_2, \phi_3\}$  of the velocity  $\{u, v, w\}$  at  $k_x = 0, k_z = 2$ . (a) First, (b) second, (c) third, (d) fourth, (e) fifth, (f) sixth.

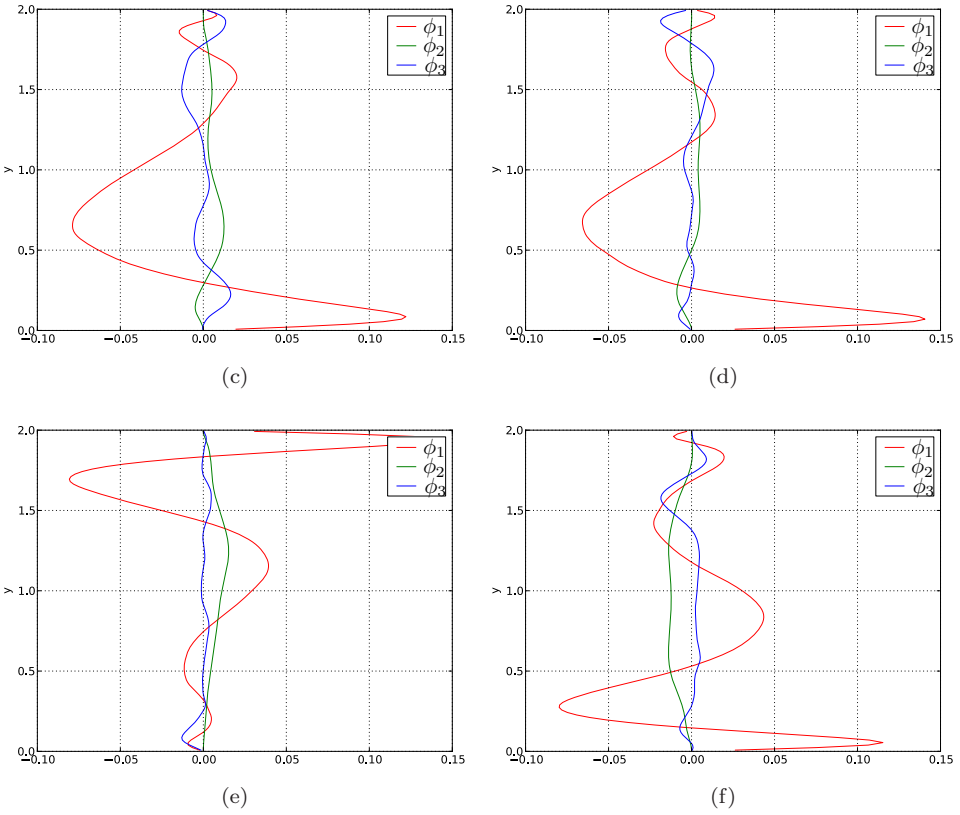


Fig. 3. (Continued)

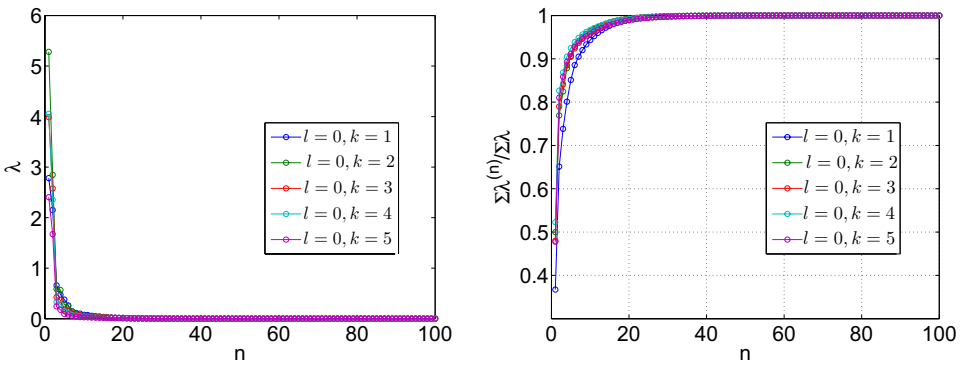


Fig. 4. Eigenvalues (left) and relative contribution of the wall-normal mode to the total kinetic energy  $\lambda_{lk}^1 / \sum_n \lambda_{lk}^{(n)}$  (right) versus the mode order  $n$  at  $(l = 0, k = 1)$ ,  $(l = 0, k = 2)$ ,  $(l = 0, k = 3)$ ,  $(l = 0, k = 4)$  and  $(l = 0, k = 5)$ .

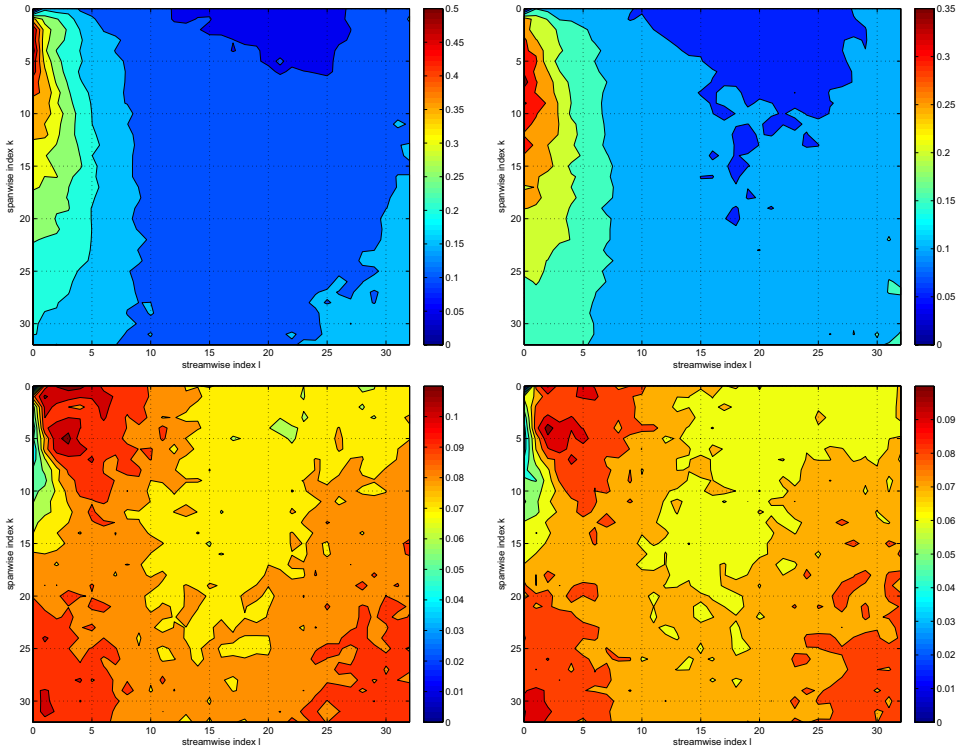


Fig. 5. Relative contribution of the first (left top), second (right top), third (left bottom) and fourth (right bottom) wall-normal mode to the total kinetic energy  $\lambda_{lk}^{(n)}/\sum \lambda_{lk}^{(n)}$  versus streamwise ( $l$ ) and spanwise ( $k$ ) wave number.

first two wall-normal eigenmodes, the contribution of the first two modes is around 80% for the low wave numbers. The portion of the total fluctuating kinetic energy contained in the first ( $\lambda_{lk}^1/\sum_n \lambda_{lk}^{(n)}$ ), second ( $\lambda_{lk}^2/\sum_n \lambda_{lk}^{(n)}$ ), third ( $\lambda_{lk}^3/\sum_n \lambda_{lk}^{(n)}$ ) and fourth ( $\lambda_{lk}^4/\sum_n \lambda_{lk}^{(n)}$ ) eigenfunction versus the streamwise and spanwise wave number are shown in Fig. 5, respectively. It can be observed that for the first two wall-normal modes the low wave numbers take dominant contributions, as the order of the wall-normal mode increases the contributions do not remain in the low wave number zone. This means if many wall-normal modes are required, a large range of spanwise and streamwise wave numbers must be included to guarantee consistency in frequency. Figure 6 shows the combined contribution of the first four wall-normal modes to the total kinetic energy  $\sum_{n=1}^4 \lambda_{lk}^{(n)}/\sum \lambda_{lk}^{(n)}$ . In spite of the energy distribution of the third and fourth wall-normal modes, overall the low wave numbers still make the dominant contributions.

All the treatments to the velocity are separately applied to the pressure. The first four modes are shown in Fig. 7. Again, the number of zero-crossing increased with the order of the eigenmodes.

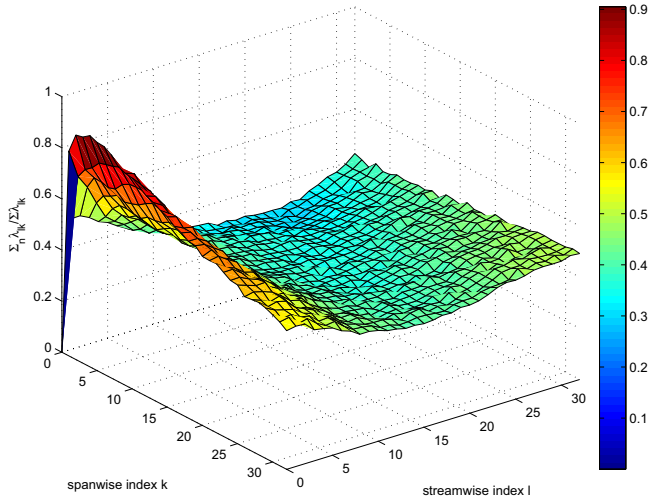


Fig. 6. Relative contribution of the first four wall-normal modes to the total kinetic energy  $\sum_{n=1}^4 \lambda_{lk}^{(n)} / \sum \lambda_{lk}$  versus streamwise and spanwise wave number.

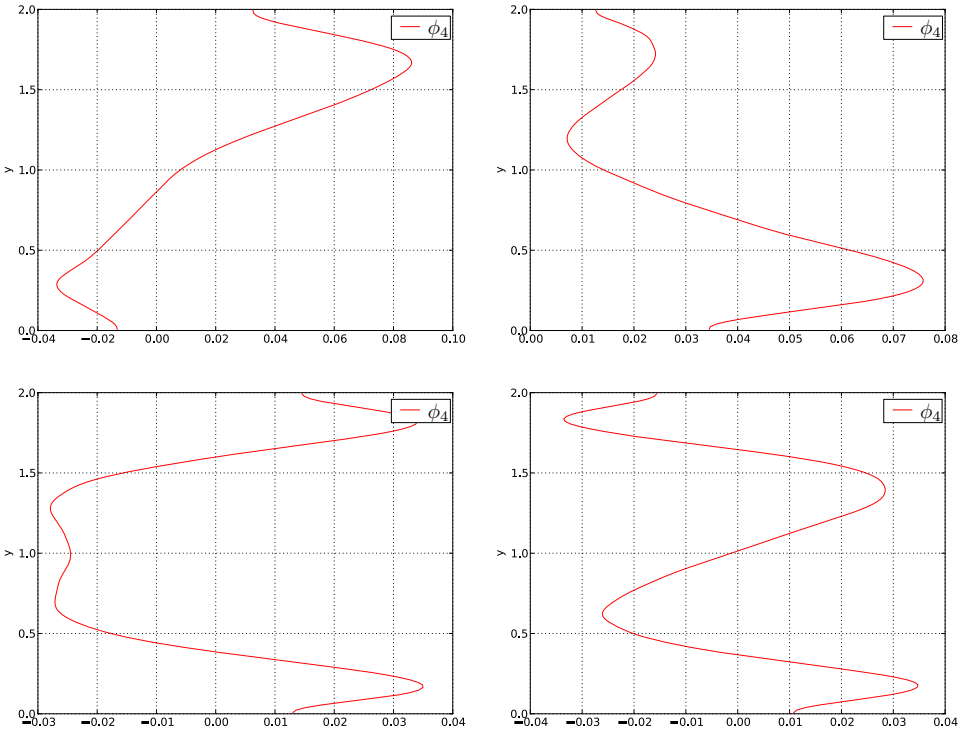


Fig. 7. The first four eigenfunctions (POD modes,  $\phi_4$ ) of the pressure ( $p$ ) at  $k_x = 0, k_z = 2$ .

### 2.3. Unresolved-scale models in VMM

The unresolved scales in the resolved-scale equations can be modeled by a standard VMM unresolved-scale model

$$U' \approx -\tau \mathcal{R}(\bar{U}), \tag{12}$$

where  $\mathcal{R}$  is a vector containing the momentum and continuity residuals of the Navier–Stokes equations, the residual-based model coefficients proposed by Taylor *et al.* [1998] are applied to  $\tau$ .

Let  $x$  denote the coordinate in the physical space, and let  $\xi$  denote the coordinate in the same point in parametric space. Let  $x = x(\xi)$  be a continuously differential map with a continuously differential inverse

$$\left(\frac{\partial x}{\partial \xi}\right)^{-1} = \frac{\partial \xi}{\partial x} \tag{13}$$

and let  $G$  be a second-rank metric tensor

$$G = \frac{\partial \xi^T}{\partial x} \frac{\partial \xi}{\partial x}. \tag{14}$$

The definition of  $\tau_M$  and  $\tau_C$  are expressed as follows.

$$\tau_M = \frac{C}{\sqrt{c_1 \bar{\mathbf{u}} \cdot G \bar{\mathbf{u}} + c_2 \nu^2 G : G + c_3 \frac{1}{\Delta t^2}}}, \tag{15}$$

$$\tau_C = \frac{\bar{\mathbf{u}} \cdot G \bar{\mathbf{u}}}{tr G}, \tag{16}$$

where  $:$  denotes a double contraction,  $C$  is a constant depending on the element topology, and  $c_1$ ,  $c_2$  and  $c_3$  are positive constants depending on the type of discretization used. This definition of  $\tau_M$  takes the orientation of the mesh with respect to the velocity into account. The approximation of the gradient and divergence operator used in the definition of  $\tau_C$  is based on kinematic considerations.

### 3. Results and Discussions

With the proposed POD-VMM technique, the LES simulations about turbulent channel flows are implemented for examining the model characteristics. As mentioned in Sec. 2.1, the mean velocity of turbulent flow is used for the resolved large scales in the simulations, while the POD modes are applied to the resolved small scales and an unresolved-scale model proposed in Taylor *et al.* [1998] is employed. It should be noted that, the truncation  $T(L, K, N)$  is defined as the set of spatial  $\phi_{lk}^n$  for POD-based model, such that  $0 \leq l \leq L$ ,  $0 \leq k \leq K$ ,  $n \leq N$ .

Previous studies claims that the first two wall-normal modes might be able to capture most of the turbulent characteristics, the feasibility of this idea has to be verified at the first beginning of our studies. Two numerical examples for testing are considered, as the first example with 481 POD modes is used with  $L = 8$ ,

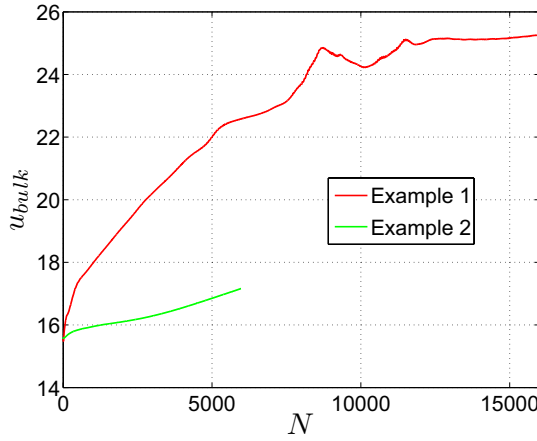


Fig. 8. Evolution of the bulk velocity  $u_{\text{bulk}}$  in time step  $tU/h$ .

$K = 12$  (Example 1), and the second one includes 1,121 modes with  $L = 15$ ,  $K = 20$  (Example 2). Figure 8 shows the evolution of the bulk velocity  $u_{\text{bulk}}$  with respect to time step  $tU/h$  of the two examples. It shows that the bulk velocity of both Example 1 sharply increases with time, but that of Example 2 increases more slowly (Example 2 is aborted earlier, as the tendency in results is already clear at time step of 6,000). The tendency of the increase in bulk velocity implies that the flow fields are “laminarizing”, that is to say, the first two wall-normal POD modes fail to capture most of the turbulent characteristics. This result can be confirmed by examining the amplitude distributions and time histories of the high-order modes, which are shown in Figs. 9 and 10. It can be seen that in both examples amplitudes of the first 200 POD mode remains fluctuating as time increases, while amplitudes of the higher order POD modes decay rapidly as time increases. It indicates that more

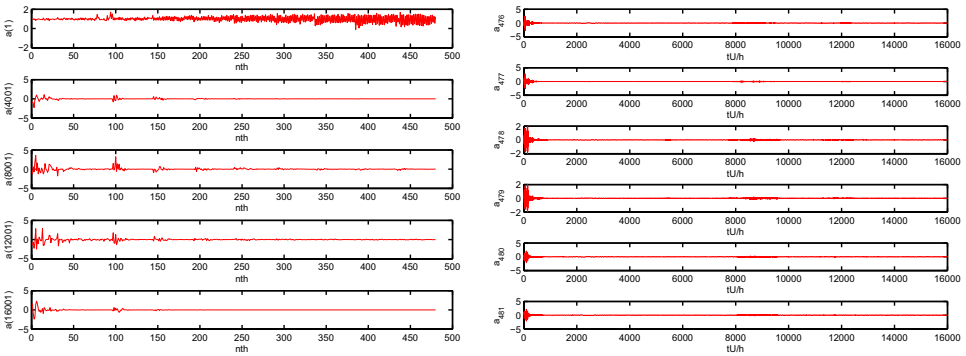


Fig. 9. Amplitude  $a(t)$  distributions of all modes (left) and time histories of the last six modes (right) of Example 1.

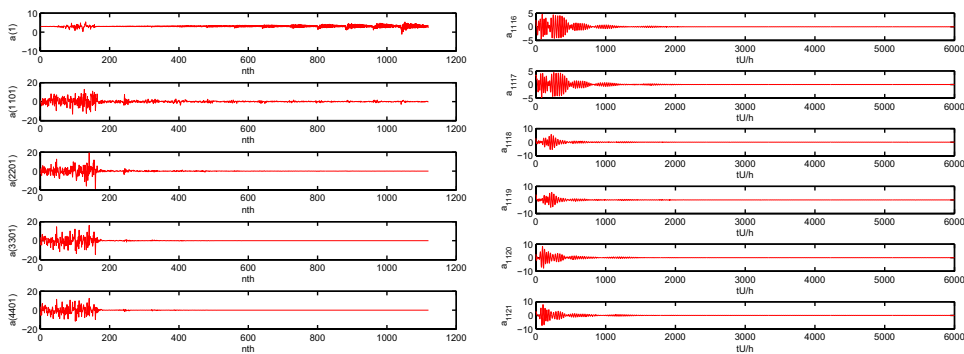


Fig. 10. Amplitude ( $a(t)$ ) distributions of all modes (left) and time histories of the last six modes (right) of Example 2.

than two wall-normal modes should be used in order to reproduce the turbulence flows.

Four wall-normal modes in the normal direction with  $L = 4$  and  $K = 10$  are then implemented to capture turbulence characteristics, which applies 400 modes in total. Notice that the modes in the normal direction increases, while the cut-off wave number in the homogeneous directions reduces. Figure 11 shows the the amplitude distributions of all modes at different time steps, from top to bottom, the increasing time steps are as 4,000, 8,000, 12,000, 16,000 and 20,000. It is of interest to notice

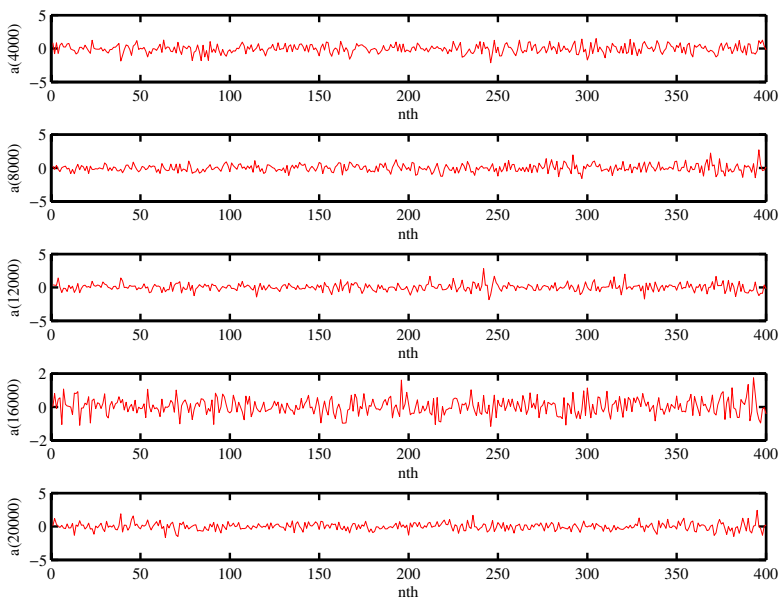


Fig. 11. Amplitudes of all modes at certain time step ( $0 \leq l \leq 4, 0 \leq k \leq 10, n \leq 4$ ).

that the amplitudes of all the modes are not constant as time step accumulates. The fluctuation of amplitude could be a sign of turbulent flow. The fluctuating behavior is also confirmed by a specific examination of the characteristics of amplitude at low- and high-order modes, as shown in Figs. 12 and 13, respectively. As the first

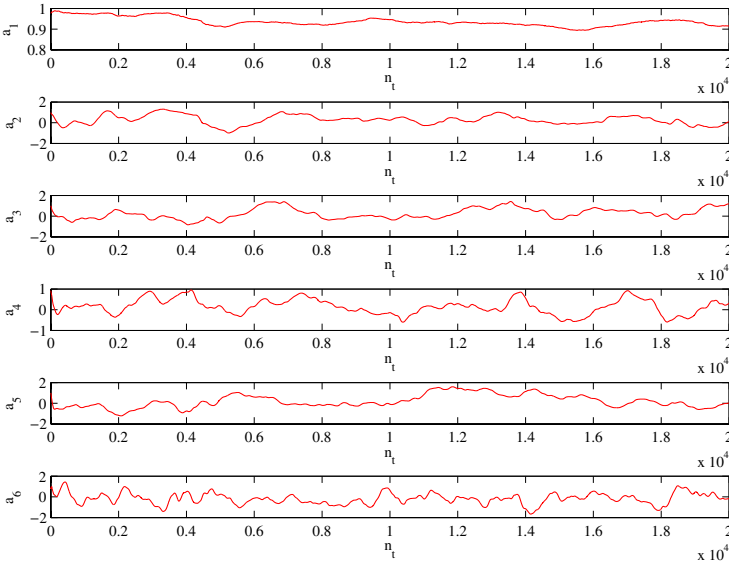


Fig. 12. Evolution of amplitudes of the first six modes ( $0 \leq l \leq 4$ ,  $0 < k \leq 10$ ,  $n \leq 4$ ).

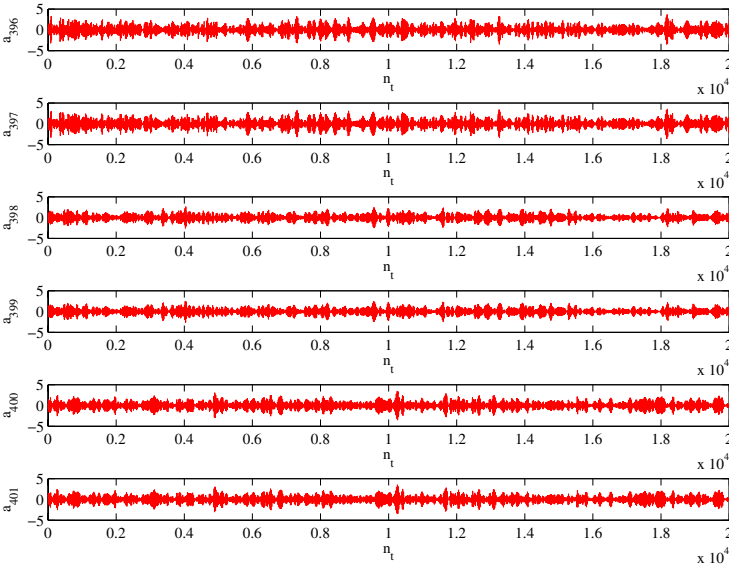


Fig. 13. Evolution of amplitudes of the last six modes ( $0 \leq l \leq 4$ ,  $0 < k \leq 10$ ,  $n \leq 4$ ).

mode denotes the mean velocity basis, it can be observed in Fig. 12, top, that the amplitude of the mean velocity basis stays between a small range from 0.95 to 1.0, which is relatively constant and confirms that the numerical simulation is stable. As the order of modes increases (from  $a_1$  to  $a_6$ ), the fluctuation of amplitude becomes obvious as expected for a turbulent simulations. Noticeably, the amplitude evolution of the low-order modes ( $a_1$ – $a_6$ ) seems to show periodic behavior, which implicitly display intermittent behavior of turbulent flows. Figure 13 shows the variations of amplitude at high-order modes (the last 6 ones) versus time step. The amplitude of high-order modes fluctuates quickly as time step increases. It is important to notice that the frequency of fluctuation of high-order modes is not only much more than that of low-order modes, but also it does not decay as the order arises. These results with four wall-normal modes confirms its feasibility in numerical simulations for turbulent characteristics.

Figure 14 shows the instantaneous isosurfaces of the streamwise velocities obtained by the LES module of OpenFOAM codes and the proposed POD-based VMM-LES approach using four wall-normal modes. The isosurfaces in a range of  $14.3 < U < 15.3$  are extracted to display the near-wall structures. Results of the widely used OpenFOAM codes (Fig. 14, left) can be applied as an reference data, in which the turbulent characteristics in both large and small scales are well simulated. According to the effects of viscosity and boundary confinement, large vortices are induced by high shear stress distributed near the boundary. The large vortices are transported by the flow in the rectangular channel, and break into several small ones in their migrating the downstream domains. Vortices are almost absent at the central area of the channel where the shear effect is vanished. These main characteristics of the turbulent flow have also been well estimated by the proposed POD-based VMM-LES approach using four wall-normal modes, such as the structure distribution of large vortices, as shown in Fig. 14 (right). A similar conclusion can be also obtained from Fig. 15, which shows the streaks of the streamwise velocity on

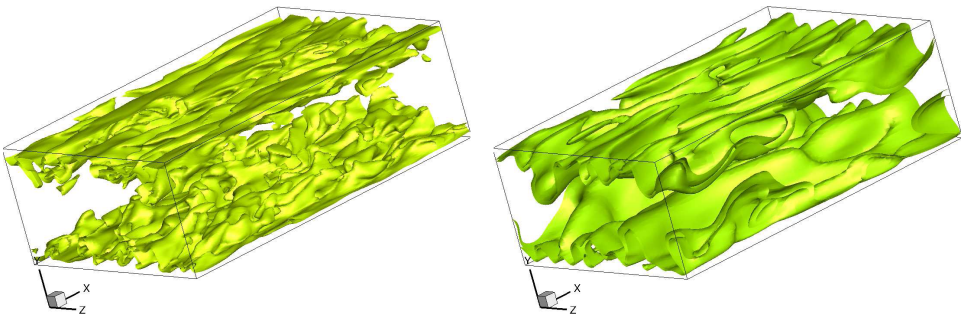


Fig. 14. Instantaneous isosurfaces of the streamwise velocity. The left figure represents the results of OpenFOAM (as a reference data), and the right one is obtained with the proposed POD-based VMM-LES approach using four wall-normal modes.

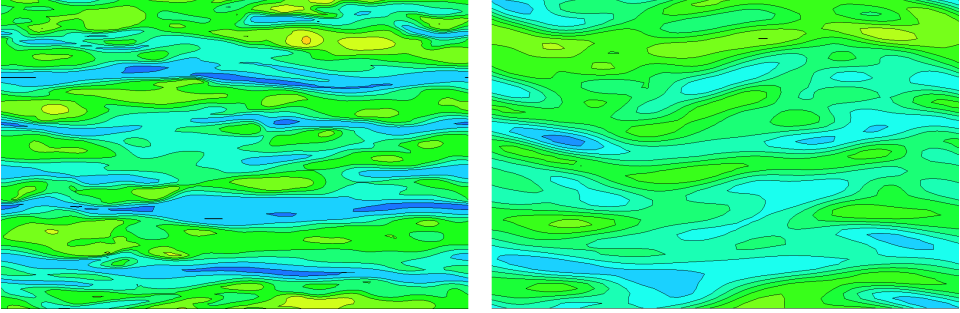


Fig. 15. Streaks of the streamwise velocity on  $xz$ -plane at  $y^+ = 10$ . The left figure represents the results of OpenFOAM (as a reference data), and the right one is obtained with the proposed POD-based VMM-LES approach using four wall-normal modes.

$xz$ -plane at  $y^+ = 10$ , obtained from the LES module of OpenFOAM codes and the present model, respectively. The two approaches have successfully presented obvious streaks in a 2D view, although the LES codes that uses more computational times can show more detail of the flow structures. Both the 3D and 2D results show that the proposed model successfully reproduces the main structures of turbulence flow, which can be very appropriate for the predications of turbulent structures with a very low cost of numerical computations.

The statistical analysis on the numerical results with the proposed POD-based VMM-LES approach using four wall-normal modes is also carried out for a better understanding of the model properties. The results of mean velocity and RMS of fluctuating velocities are shown in Fig. 16, where the results of present model are compared with the published DNS results in Jimenez and Moser [2007]. The mean velocities obtained by present approach, as shown in the left-top of Fig. 16, are in a good agreement with that of Jimenez's DNS results, especially in the range of  $y^+ = 1-30$  which denotes the location near the boundary (inner layer). Although small deviation still exists for the outer layer ( $y^+ > 30$ ), the predicated RMS of fluctuating velocities in the normal and spanwise directions ( $v_{\text{rms}}$  and  $w_{\text{rms}}$ ) by present approach coincide well with that of Jimenez's DNS results, as shown in the right-top and left-bottom of Fig. 16, respectively. It is of interest to notice that a deviation between the two results still exists in the results on the streamwise direction ( $u_{\text{rms}}$ ), which implies that the increase of POD modes could be necessary if a precise result on streamwise direction is required.

The distribution of Reynolds stress ( $-u'v'$ ) of turbulent flows in  $y$ -direction is presented in Fig. 17. The Reynolds stress ( $-u'v'$ ) obtained by present approach differs from Jimenez's DNS results in the range of  $y = 0.1-0.6$ , even if they coincide with each other in the other part. It results from the difference of fluctuating velocities between present model and Jimenez's DNS results on the streamwise direction, as mentioned above. It implies that, more wall-normal modes need to be adopted in the POD-based VMM-LES technique to achieve more precise results of Reynolds

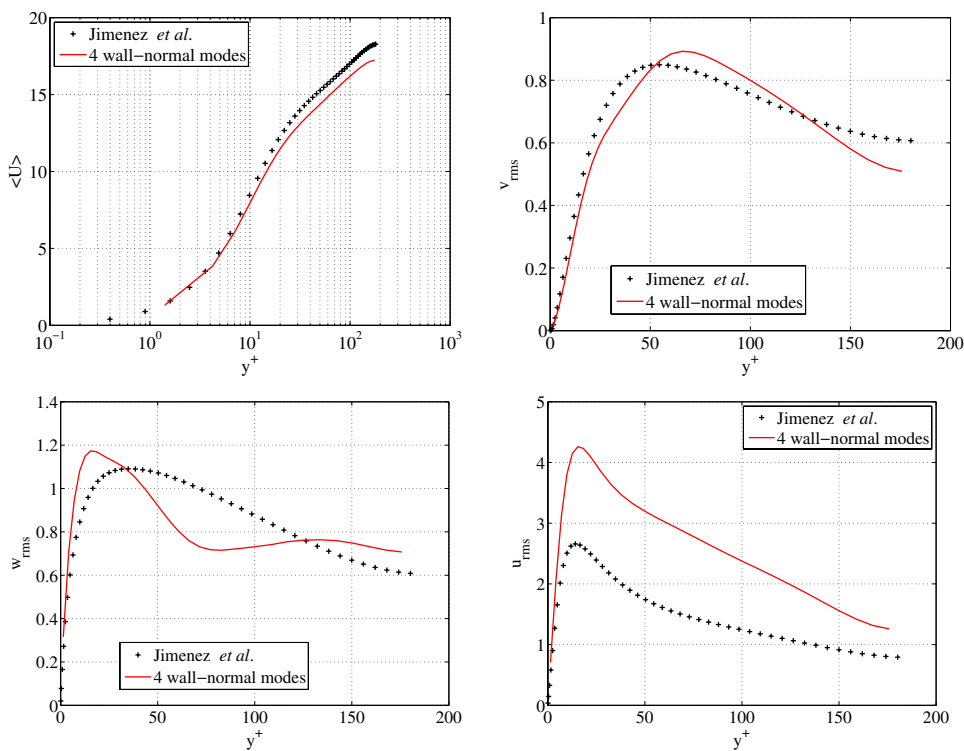


Fig. 16. Statistical results of the mean velocity (left top) and RMS of fluctuating velocities (the other three ones).

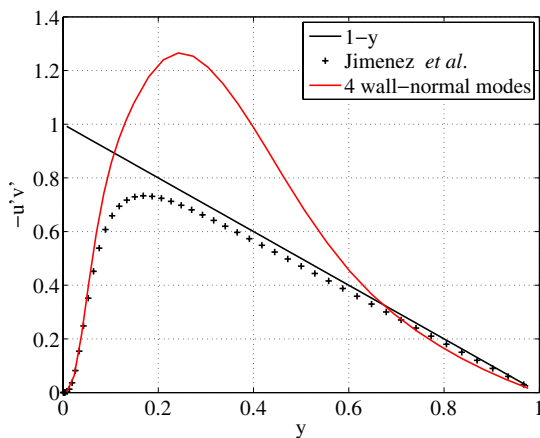


Fig. 17. The distribution of Reynolds stress  $(-u'v')$  of turbulent flows in  $y$ -direction.

stress, as well as the fluctuating velocities on streamwise direction. This can be an interesting point to be verified in our future study.

#### 4. Conclusions

A POD-based VMM for LES of turbulent channel flows was proposed in this study. We applied the residual-based VMM technique to solve the incompressible Navier–Stokes equations. For the temporal integration, a generalized- $\alpha$  method is used. The residual-based model coefficient proposed by Taylor *et al.* [1998] was employed in the present model. Validation of the POD modes and careful analysis on the model properties were presented. Numerical implementations on the turbulent channel flows were performed, and the numerical results of turbulent structures and the statistical analysis were well organized with careful discussions, by the comparisons to some classical published LES/DNS results. The main findings in present study can be summarized as follows:

- (1) The fluctuation of high-order modes, in the proposed POD-based VMM-LES technique using two wall-normal modes, decays as the numerical time step accumulates, while it remains fluctuating for that using four wall-normal modes. Four or higher wall-normal modes need to be used to reproduce the turbulent characteristics.
- (2) The numerical results of structure distribution of large vortices and low velocity streaks both demonstrate that the turbulent channel flow are well estimated by the proposed approach using four wall-normal modes.
- (3) The statistical results of turbulent channel flows obtained from the present simulations are in a good agreement with previous LES/DNS results.

In summary, the reliability and feasibility of proposed POD-based VMM-LES approach are confirmed by numerical implementations and statistical analysis. It demonstrates that the proposed approach can efficiently and precisely simulate the turbulent characteristics using Four wall-normal modes, especially for the large scale structures. According to the present results, more modes are suggested to capture the flow features at small scales, even if it is at the cost of more computational time. A further study on the effect of higher wall-normal modes is still left for our future work.

#### Acknowledgments

This project was supported by the National Natural Science Foundation of China (No. 11402084), the Natural Science Foundation of Hunan Province (No. 2015JJ3051), the self-determined project of State Key Laboratory of Advanced Design and Manufacturing for Vehicle Body (No. 51475002) and the Fundamental Research Funds for the Central Universities (Hunan University). The academic visits of Dr. L.-F. Chen to Changsha are supported by the Fundamental Research Funds for the Central Universities (Hunan University).

## References

- Amsallem, D., Cortial, J., Carlberg, K. and Farhat, C. I. [2009] “A method for interpolating on manifolds structural dynamics reduced-order models,” *Int. J. Numer. Methods Eng.* **80**(9), 1241–1258.
- Aubry, N., Holmes, P., Lumley, J. L. and Stone, E. [1988] “The dynamics of coherent structures in the wall region of a turbulent boundary layer,” *J. Fluid Mech.* **192**, 115–173.
- Bakewell, H. P. and Lumley, J. L. [1967] “Viscous sublayer and adjacent wall region in turbulent pipe flow,” *Phys. Fluids* **10**(9), 1880–1889.
- Ball, K. S., Sirovich, L. and Keefe, L. R. [1991] “Dynamical eigenfunction decomposition of turbulent channel flow,” *Int. J. Numer. Methods Fluids* **12**(6), 585–604.
- Bazilevs, Y., Calo, V. M., Cottrell, J. A., Hughes, T. J. R., Reali, A. and Scovazzi, G. [2007] “Variational multiscale residual-based turbulence modeling for large eddy simulation of incompressible flows,” *Comput. Methods Appl. Mech. Eng.* **197**(1–4), 173–201.
- Calo, V. [2005] “Residual-based multiscale turbulence modeling: Finite volume simulations of bypass transition,” PhD thesis, Stanford, CA, USA.
- Chen, L., Edeling, W. N. and Hulshoff, S. J. [2015] “POD enriched boundary models and their optimal stabilisation,” *Int. J. Numer. Methods Fluid* **77**(2), 92–107.
- Hughes, T. J. R. and Sangalli, G. [2007] “Variational multiscale analysis: The finescale greens function, projection, optimization, localization, and stabilized methods,” *SIAM J. Numer. Anal.* **45**(2), 539–557.
- Hughes, T. J. R., Mazzei, L. and Jansen, K. E. [2000] “Large eddy simulation and the variational multiscale method,” *Comput. Vis. Sci.* **3**, 47–59.
- Hughes, T. J. R., Mazzei, L., Oberai, A. A. and Wray, A. A. [2001a] “The multi-scale formulation of large eddy simulation: Decay of homogeneous isotropic turbulence,” *Phys. Fluids* **13**(2), 505–512.
- Hughes, T. J. R., Oberai, A. A. and Mazzei, L. [2001b] “Large eddy simulation of turbulent channel flows by the variational multiscale method,” *Phys. Fluids* **13**(6), 1784–1799.
- Jimenez, J. and Moser, R. D. [2007] “What are we learning from simulating wall turbulence?” *Phil. Trans. R. Soc. A: Math. Phys. Eng. Sci.* **365**(1852), 715–732.
- Lumley, J. L. [1967] “The structure of inhomogeneous turbulent flows,” in *Atmos. Turbulence and Radio Propagation*, House “Nauka”, pp. 166–178.
- Moin, P. and Moser, R. D. [1989] “Characteristic-eddy decomposition of turbulence in a channel,” *J. Fluid Mech.* **200**, 471–509.
- Sirovich, L. [1991] “Empirical eigenfunctions and low dimensional systems,” in *New Perspectives in Turbulence* (Springer), pp. 139–163.
- Taylor, C. A., Hughes, T. J. R. and Zarins, C. K. [1998] “Finite element modeling of blood flow in arteries,” *Comput. Methods Appl. Mech. Eng.* **158**(1–2), 155–196.
- Wang, Z., Akhtar, I., Borggaard, J. and Iliescu, T. [2012] “Proper orthogonal decomposition closure models for turbulent flows: A numerical comparison,” *Comput. Methods Appl. Mech. Eng.* **237**, 10–26.
- Wei, Y. K. and Hu, X. Q. [2016] “Two-dimensional simulations of turbulent flow past a row of cylinders using lattice Boltzmann method,” *Int. J. Comput. Methods*, 1750002.